Applied Surface Science 284 (2013) 849–854

Contents lists available at ScienceDirect

Applied Surface Science

journal homepage: www.elsevier.com/locate/apsusc

The improved performance of solution-processed SQ:$PC_{71}BM$ photovoltaic devices via MoO_3 as the anode modification layer

Qianqian Yang[a,b], Daobin Yang[c], Suling Zhao[a,b,*], Yan Huang[c,**], Zheng Xu[a,b], Xiaodong Liu[a,b], Wei Gong[a,b], Xing Fan[a,b], Qingyu Huang[a,b], Xurong Xu[a,b]

[a] Key Laboratory of Luminescence and Optical Information, Beijing Jiaotong University, Ministry of Education, Beijing 100044, China
[b] Institute of Optoelectronics Technology, Beijing Jiaotong University, Beijing 100044, China
[c] College of Chemistry, Sichuan University, Chengdu 610064, China

ARTICLE INFO

Article history:
Received 25 May 2013
Received in revised form 11 July 2013
Accepted 6 August 2013
Available online 16 August 2013

Keywords:
Organic photovoltaic devices
Solution-processed
Anode modification
MoO_3
Thermal annealing

ABSTRACT

The enhanced performance of a squaraine compound, 2,4-bis[4-(N,N-diisobutylamino)-2,6-dihydroxyphenyl] squaraine (SQ) as a donor, and [6,6]-phenyl-C71-butyric acid methyl ester ($PC_{71}BM$) as an acceptor in solution processed organic photovoltaic devices (OPVs) via the anode modification and thermal annealing is investigated. Through the optimization of these two factors, a maximum power conversion efficiency (PCE) of 4.08% under AM 1.5 G illumination (100 mW/cm^2) is obtained. The results show that poly (3,4-ethylenedioxythiophene):poly (styrenesulfonicacid) (PEDOT:PSS) deteriorates the performance of SQ:$PC_{71}BM$ based OPVs, and MoO_3 is used to substitute PEDOT:PSS as an effective exciton-blocking layer. A higher open-circuit voltage (V_{OC}) of 0.95 V is reached. The barrier matching between the energy-level of MoO_3 and HOMO of SQ enhances fill factor (FF) and short-circuit current density (J_{SC}). The operation mechanism of the thermal annealing is also straightened out. The higher carrier mobility and improved contact is obtained under 70 °C annealing, which results from the higher nanoscale crystallinity and the optimal scale phase separation between donor–acceptor networks. Hence the balanced charge carrier mobility increases the FF and PCE of OPVs by decreasing the charge recombination.

1. Introduction

Organic photovoltaic devices (OPVs) have attracted great research interest due to their potential as lightweight, low-cost, flexible sources of renewable energy [1–3]. Although encouraging progress has been made in recent years, it has still not approached commercialization compared to silicon based solar cells. The power conversion efficiency (PCE) of OPVs needs to be increased further to satisfy the practical applications. So far, both solution process and thermal evaporation are used to fabricate OPVs. Solution process has been more widely used due to the easy operation and the potentially low-cost of fabrication [4,5]. To obtain improved performance, efforts have focused on the design and synthesis of soluble donors with high charge carrier mobility and absorption in the visible and new-infrared spectral regions, in combination with the high interfacial gap energy at the donor–acceptor interface. Among the small molecule materials, owing to their high absorption coefficients and intense absorption in the red and near-infrared (NIR) spectral regions, 2,4-bis[4-(N,N-diisobutylamino)-2,6-dihydroxyphenyl] squaraine (SQ) dyes have shown tremendous potential for OPVs [6–8]. Especially, SQ has lower highest occupied molecular orbits (HOMO) energy level than that of other commonly used donors such as copper phthalocyanine [9].

The device performances of OPVs are greatly dependent on the properties of active layer materials, nanoscale morphology, and interface modification. Anode modification and thermal annealing have been demonstrated as the efficient ways to improve the PCE of OPVs. In order to modify the interface between active layer/anode, many buffer layers or ultrathin layers have been reported, such

* Corresponding author at: Key Laboratory of Luminescence and Optical Information, Beijing Jiaotong University, Ministry of Education, Beijing 100044, China. Tel.: +86 010 51688675.
** Corresponding authorat: College of Chemistry, Sichuan University, Chengdu 610064, China. Tel.: +86 028 85410059.
E-mail addresses: 10118387@bjtu.edu.cn (Q. Yang), 13408096284@163.com (D. Yang), slzhao@bjtu.edu.cn (S. Zhao), huangyan@scu.edu.cn (Y. Huang), zhengxu@bjtu.edu.cn (Z. Xu), 08118347@bjtu.edu.cn (X. Liu), 08122219@bjtu.edu.cn (W. Gong), 10118386@bjtu.edu.cn (X. Fan), 12118413@bjtu.edu.cn (Q. Huang), xrxu@bjtu.edu.cn (X. Xu).

0169-4332
http://dx.doi.org/10.1016/j.apsusc.2013.08.020

as poly (3,4-ethylenedioxythiophene):poly (styrenesulfonicacid) (PEDOT:PSS) [10], NiO [11], MoO_3 [12–14], WO_3 [15], and V_2O_5 [12]. Especially, PEDOT:PSS is the best popular anode modification material. However, it is also found that PEDOT:PSS deteriorates the device performance [16,17]. On the other hand, thermal annealing has been demonstrated as an efficient way to improve the performance in OPVs [18,19]. Using these methods, a bulk heterojunction (BHJ) with a preferred donor domain size and bicontinuous interpenetration network is formed, which allows the excitons to diffuse to the donor–acceptor interface and charge carriers to transport to the respective electrodes after separation.

In this work, we demonstrate that the performance of solution-processed SQ:$PC_{71}BM$ based small molecule organic solar cells can be improved via anode modification and thermal annealing methods. MoO_3 was used to substitute PEDOT:PSS as the anode modification layer and the influence of acidic interlayer (PEDOT:PSS) on the performance of OPVs was investigated in detail. The morphology and charge carrier mobility of SQ:$PC_{71}BM$ films were characterized to illuminate the mechanism of thermal annealing.

2. Experimental

Patterned indium tin oxide (ITO)-coated glass substrates with a sheet resistance of 15 ohm/square were cleaned consecutively in ultrasonic bath containing detergent, acetone, ethanol, and deionized water for 10 min each, and finally blow-dried by high purity nitrogen. The substrates were treated by UV-ozone for 5 min, and then the buffer layer was fabricated. For the buffer layer, two different materials were used, namely, PEDOT:PSS and MoO_3. A PEDOT:PSS layer of about 25 nm thickness was obtained by spin-coating an aqueous solution (Clevios P Al 4083) onto ITO coated glass substrates, followed by baking at 120 °C for 10 min. 80 Å MoO_3 layer was thermally evaporated onto ITO substrates under a vacuum of less than 3×10^{-4} Pa at a rate of 0.5 Å/s. Subsequently, the photoactive layer was fabricated by spin-coating a blend of the SQ and $PC_{71}BM$ in chloroform with total concentration of 20 mg/mL (1500 rpm, 50 s) under a N_2-filling glove box at 25 °C. The solution mixture was stirred for 12 h at room temperature. Then the substrates were loaded into a vacuum chamber to deposit LiF (8 Å) and Al (1000 Å) under a pressure of less than 3×10^{-4} Pa at a rate of 0.2 Å/s and 1.5 Å/s respectively. Deposition rate and film thickness were in situ monitored using a quartz crystal oscillator mounted to the substrate holder. The active area is 6 mm^2. The current–voltage curves in dark and under illumination were measured using an Abet solar simulator with a Keithley 4200 source measurement unit under AM 1.5 G illumination (100 mW/cm^2), after spectral mismatch correction under an ambient atmosphere at 25 °C. The absorption spectrum was measured by Shimadzu UV-3101 PC spectrometer under an ambient atmosphere at 25 °C. Thermal annealing was carried out by directly placing the substrates with spin coated photoactive layers on a digitally controlled hotplate at various temperatures for 10 min in a N_2-filling glove-box. Hole-only devices were fabricated with the structure of ITO/MoO_3 (8 nm)/SQ:$PC_{71}BM$ (80 nm)/Au (100 nm). Samples for atomic force microscopy (AFM) measurements were prepared by casting SQ:$PC_{71}BM$ blend thin films on ITO-coated glass substrates with a 8 nm thick MoO_3. The chemical structure of SQ and device structure of OPVs is shown in Fig. 1(a). The energy level diagrams of different materials used in the device fabrication are shown in Fig. 1(b).

3. Results and discussion

Fig. 2 shows the current density–voltage (*J*–*V*) characteristics of different OPVs under AM 1.5 G illumination with an intensity of 100 mW/cm^2. For the ITO only device, the PCE is only 2.84% due

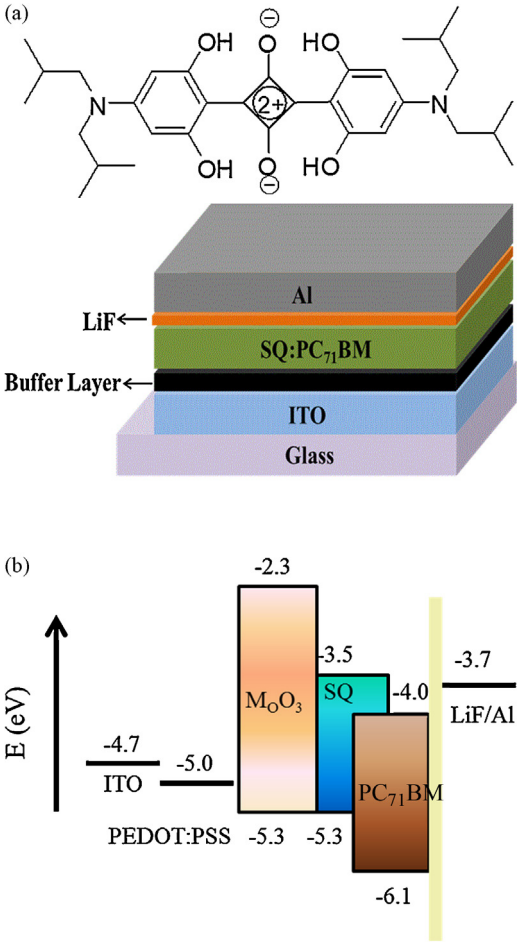

Fig. 1. (a) Chemical structure of SQ and device structure of OPVs. (b) Energy level diagram of OPVs.

to the low fill factor (FF) of 36%, despite the high short-circuit current density (J_{SC}) of 8.76 mA/cm^2 and the high open-circuit voltage (V_{OC}) of 0.90 V. The V_{OC} and FF of the device with MoO_3 as a buffer layer inserted between ITO and the photoactive layer increases to 0.95 V and 43%, respectively, and J_{SC} of this device is 8.79 mA/cm^2, almost unchanged compared with that of the ITO only device. Therefore, the PCE of the device with MoO_3 buffer layer increases to 3.59%. Using the more widely used PEDOT:PSS interlayer leads to a diminished performance, particularly a loss in V_{OC}. The PCE of the device with PEDOT:PSS interlayer is less than 2.0%, with the J_{SC} of 7.90 mA/cm^2, V_{OC} of 0.79 V and FF of 31%. We also prepared conventional devices based on poly(3-hexylthiophene):(6,6)-phenyl C_{61} butyric acid methyl ester (P3HT:$PC_{61}BM$) with two different buffer layers, MoO_3 and PEDOT:PSS. *J*–*V* characteristics are shown in Fig. 2(b). It shows that V_{OC} of two devices are almost same, and the performances change a little. Thus we believe that PEDOT:PSS buffer layer in SQ:$PC_{71}BM$ based OPVs must involve a different mechanism from it in conventional P3HT:$PC_{61}BM$ based OPVs (Table 1).

The diminished performance can be explained by the protonation of the pyridyl nitrogen due to the strong acidic nature of PEDOT:PSS, like p-DTS($PTTh_2$)$_2$ [20]. To explore whether SQ molecules are sensitive to protonation, the solution absorption spectra of SQ with various equivalents of trifluoroacetic CF_3CO_2H acid in chloroform are measured. The resulting absorption profiles (Fig. 3(a)) show significant changes immediately upon acid addition. A new peak around 530 nm is detected but the absorption around 690 nm decreases. It suggests that the chromophore

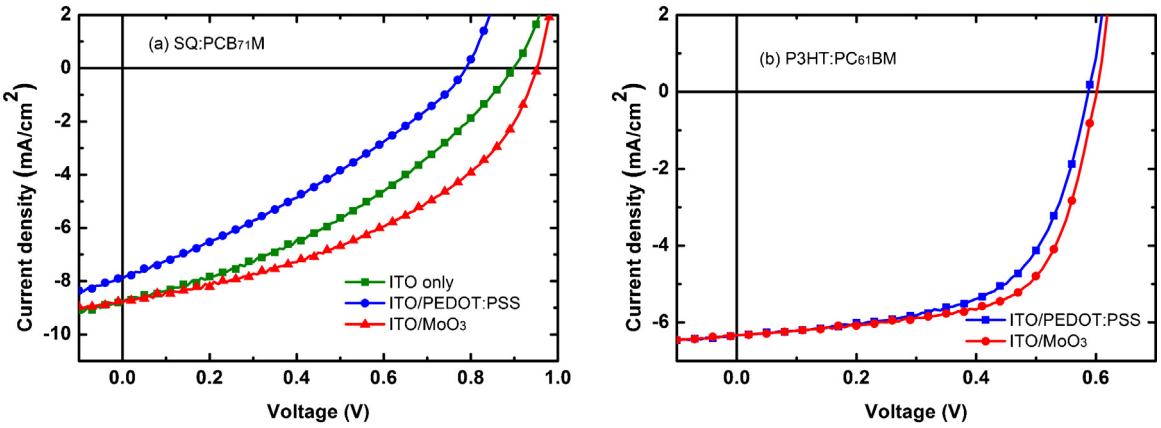

Fig. 2. *J–V* characteristics of OPVs with different types of anodes, namely, ITO only, ITO with PEDOT:PSS, and ITO with MoO_3 (8 nm): (a) SQ:PC_{71}BM blend and (b) P3HT:PC_{61}BM blend.

backbone is influenced by the protonation. Notably, the effect does not saturate even up to ten equivalents of acid, which means an equilibrium between protonated and non-protonated species in solution. Above results indicate that SQ is sensitive to acidic condition and the acidic buffer layer can cause performance degradation in SQ based OPVs.

To confirm our ideas, we further investigate the absorption spectra of SQ:PC_{71}BM blend films with different buffer layers (ITO/PEDOT:PSS and ITO/MoO_3) before and after keeping the blend films in the N_2-filling glove box for 48 h. All the absorption spectra are shown in Fig. 3(b). The major peak at 690 nm originates from SQ. After the blend films are kept in the N_2-filling glove box for 48 h, the intensities of the peak at 690 nm decrease for both kinds of anode buffer layers but in the case of PEDOT:PSS, the intensity declines more obviously. This demonstrates that PEDOT:PSS can undergo chemical reaction with SQ and leads to an instability of the photoactive layer. Therefore, the performance of SQ:PC_{71}BM solar cells declines rather than improves after introducing the PEDOT:PSS buffer layer.

Table 1
Photovoltaic performance parameters of OPVs with different types of anodes.

Anode	V_{OC} (V)	J_{SC} (mA/cm^2)	FF	PCE (%)
ITO only	0.90	8.76	0.36	2.84
ITO/PEDOT:PSS	0.79	7.90	0.31	1.93
ITO/MoO_3	0.95	8.79	0.43	3.59
P3HT reference ITO/PEDOT:PSS	0.59	6.33	0.60	2.24
P3HT reference ITO/MoO_3	0.60	6.33	0.65	2.47

Considering that PEDOT:PSS causes the deterioration of the photoactive layer, MoO_3 is used to modify the anode in SQ:PC_{71}BM based solar cells. With the insertion of MoO_3 layer, the performance is remarkably improved. It can be explained by the proper energy-level alignment between MoO_3 and SQ, which results in the efficient hole extraction. In addition, the band gap of MoO_3 is around 3 eV. MoO_3 can act as an effective exciton-blocking layer to mainly prevent exciton quenching at the anode.

On the other hand, V_{OC} of the device increases from 0.9 V to 0.95 V after MoO_3 modification. The higher V_{OC} can be expected according to the Shockley equation as a consequence of reduced leakage current (Fig. 4). The Shockley equation is given by

$$V_{OC} = \frac{nkT}{q}\left(\ln\frac{J_{ph}}{J_S} + 1\right) \quad (1)$$

where J_{ph} is the photocurrent, J_S is the reverse dark saturation current density, n is the ideality factor, k is the Boltzmann constant and q is the elementary charge. In general, the decreasing dark current density J_D and a decreasing reverse dark saturation current density J_S help to enhance V_{OC} of the devices [21].

What's more, according to the model of Mihailetchi et al. [22], the dark *J–V* characteristics of solar cells can be split into three distinct regimes: a leakage current dominated regime at low voltages, a diffusion current dominated regime around the built-in voltage, and a space charge limited current dominated regime at high voltages. As shown in Fig. 4, in the leakage dominated regime (<0.9 V),

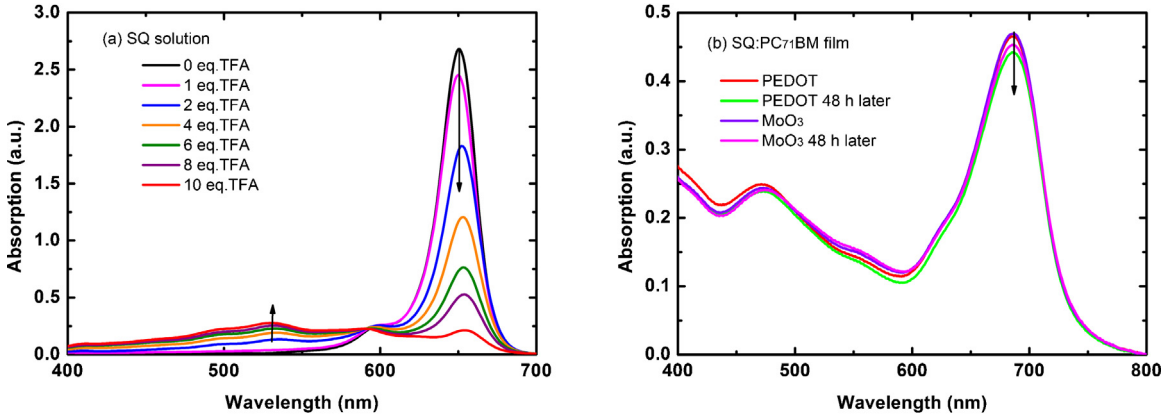

Fig. 3. Absorption spectra of (a) SQ with various equivalents of trifluoroacetic acid in chloroform. (b) SQ:PC_{71}BM blend films with different types buffer layers and then kept in the N_2-filling glove box for 48 h later.

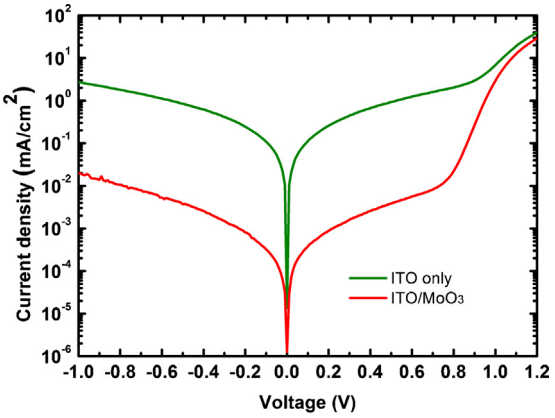

Fig. 4. Semi-logarithmic current density vs. voltage characteristics of ITO only and ITO/MoO_3 devices in the dark.

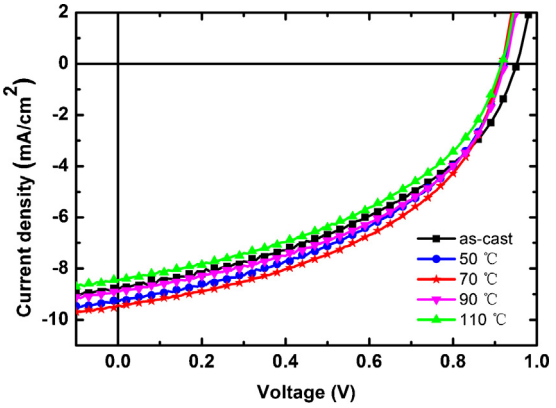

Fig. 6. *J–V* characteristics of OPVs based on SQ:$PC_{71}BM$ blend films with various annealing temperatures for 10 min.

the dark current density of the device with a MoO_3 interlayer is 1–2 orders lower than that of the ITO only device. The V_{OC} increment is calculated to be 0.05–0.10 V by using Eq. (1) according to J_D value in this regime, which is consistent with the experimental values. However, the absolute calculated V_{OC} is not available since the Shockley model is not an accurate model for BHJ devices. It also be noted that the diffusion current dominated regime shifts 50 mV in the device with MoO_3 interlayer compared to that of ITO only device, which is strong evidence that the built-in voltage of the active layer can indeed be enhanced by MoO_3 interlayer.

Fig. 5 shows the external quantum efficiency (EQE) of the corresponding OPVs. For the entire wavelength range, the EQE spectra consist of three major peaks at approximately 360 nm, 480 nm and 690 nm. The peaks at 360 nm and 480 nm correspond to the absorption of $PC_{71}BM$, and the third one at 690 nm arises from SQ. The device with MoO_3 layer exhibits a higher EQE than that of the other two. In addition, there is no noticeable difference in shape of the EQE spectra between ITO only and ITO/MoO_3 devices. But for ITO/PEDOT:PSS device, the EQE peak of SQ decreases more pronouncedly than the other two peaks of $PC_{71}BM$. These results, directly analogous to those obtained in absorption, further confirm above discussions. Therefore, it is concluded that MoO_3 is favorable to improve the performance of SQ:$PC_{71}BM$ based solar cells. In order to get an enhanced performance, the thermal annealing for SQ:$PC_{71}BM$ film at various temperatures was processed.

The *J–V* characteristics of OPVs based on SQ:$PC_{71}BM$ blend films with various annealing temperatures from 50 °C to 110 °C for 10 min in nitrogen are exhibited in Fig. 6. The extracted device parameters are summarized in Table 2. As illustrated in Fig. 6, V_{OC} remains almost unchanged for all devices, whereas J_{SC} and FF firstly increase and then decrease when the treatment temperature is higher than 70 °C. J_{SC} reaches a maximum value of 9.44 mA/cm^2 after annealing at 70 °C, a maximum PCE of 4.08% with V_{OC} = 0.92 V and FF = 0.47 is obtained.

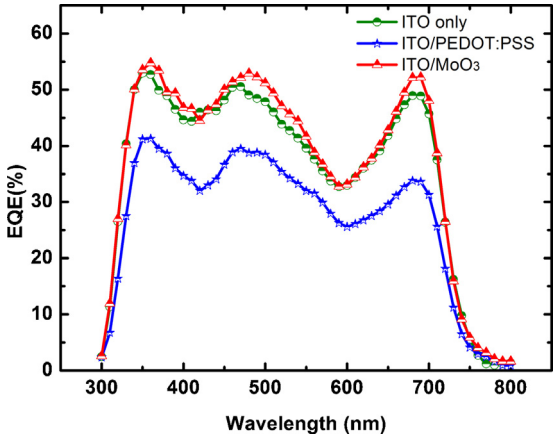

Fig. 5. External quantum efficiency as a function of wavelength for devices with various anodes.

The increase in J_{SC} and FF implies lower series resistance (R_S) and higher carrier mobility. As discussed above (shown in Table 2), the series resistance decreases from an initial value of R_S = 11.32 Ω cm^2 to R_S = 8.99 Ω cm^2 after annealing at 70 °C. In order to verify the hole-transporting properties, hole-only devices were fabricated with the structures of ITO/MoO_3/SQ:$PC_{71}BM$/Au. We measured *J–V* characteristics of the devices and then fit the results by using space-charge-limited current (SCLC) model [23–25] and the Mott–Gurney law [26] that includes field-dependent mobility. The current density is given by

$$J = \frac{9}{8}\varepsilon_0\varepsilon_r\mu\frac{V^2}{L^3} \quad (2)$$

where ε_0 is the permittivity of free-space, ε_r is the relative dielectric constant of the active layer, L is the thickness of the active layer, and μ is the zero-field mobility. The *J–V* characteristics of the devices are shown in Fig. 7. The data follow the relation of $J \propto V^2$, and hence are fitted by the SCLC model to get the value of μ_h. The results show that the hole mobility μ_h increases from 2.26×10^{-6} cm^2/V s to 3.34×10^{-6} cm^2/V s when the device annealed at 70 °C for 10 min. It suggests that the charge transport properties are substantially improved.

The higher carrier mobility of these blend films after thermal annealing is resulted from the improved nanoscale crystallinity and optimal scale of the phase separation between the donor–acceptor networks. The improved crystallization by annealing was observed in both polymer and small-molecule solar cells [18,19]. The enhanced crystallization increases the probability of optically active π–π* electronic transitions [27], so a strengthened absorption intensity can be observed. The EQE for devices annealed at various temperatures are shown in Fig. 8. The EQE peak at

Table 2
Photovoltaic performance parameters of OPVs based on SQ:$PC_{71}BM$ blend films with various annealing temperatures for 10 min.

Annealing temperature (°C)	V_{OC} (V)	J_{SC} (mA/cm^2)	FF	PCE (%)	R_S (Ω cm^2)
As-cast	0.95	8.79	0.43	3.59	11.32
50	0.92	9.28	0.45	3.84	9.48
70	0.92	9.44	0.47	4.08	8.99
90	0.92	8.90	0.46	3.77	9.87
110	0.92	8.45	0.44	3.42	10.29

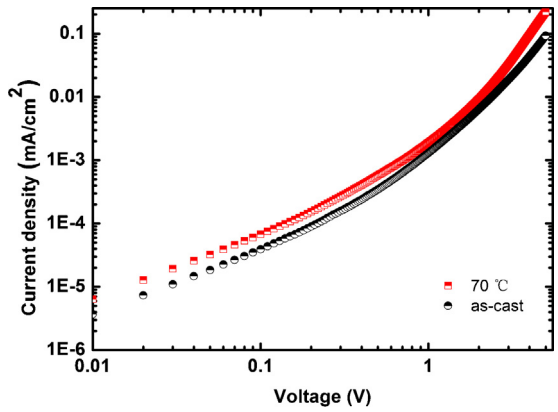

Fig. 7. *J–V* characteristics of SQ:$PC_{71}BM$ (1:5) single carrier devices used for hole mobility measurement.

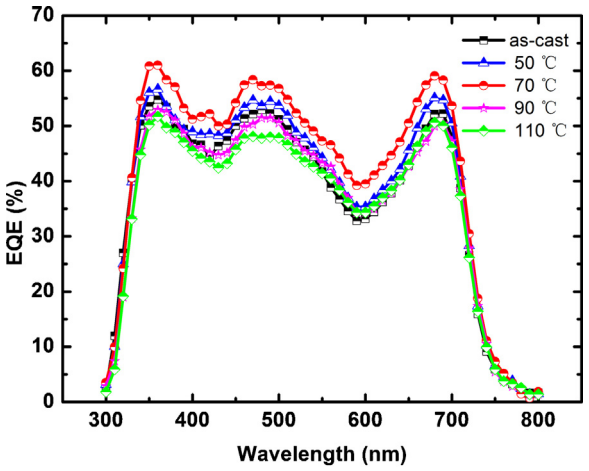

Fig. 8. External quantum efficiency as a function of wavelength for devices annealed at various temperatures for 10 min.

around 690 nm of SQ increases from 55% (as-cast) to 60% after the device annealed at 70 °C for 10 min. When the temperature further increased to 110 °C, the peak EQE is reduced to <50% across the entire wavelength range. The shape of the EQE spectrum resembles the shape of the absorption spectrum of the blended films. So the remarkable increased EQE indicates the higher absorption intensity which due to the enhanced crystallization of SQ in annealing process.

The nanoscale morphology control of the donor–acceptor interpenetrating networks by thermal annealing can be deeply understood with respect to the surface of the devices. The root-mean-square (RMS) roughness, which is in part due to the phase separation, has been observed in the AFM. The roughness obtained from the AFM images (Fig. 9(a)) of the un-annealing SQ:$PC_{71}BM$ blend films is 1.41 nm. In contrast, the roughness of the blend film annealed at 70 °C for 10 min in nitrogen increases to 3.97 nm (Fig. 9(b)). This enhanced roughness results in optimized and stable phase separation for efficient charge separation and transport. It also indicates that the annealing could lead to stronger contacts and increased contact area, which is good for the excitons

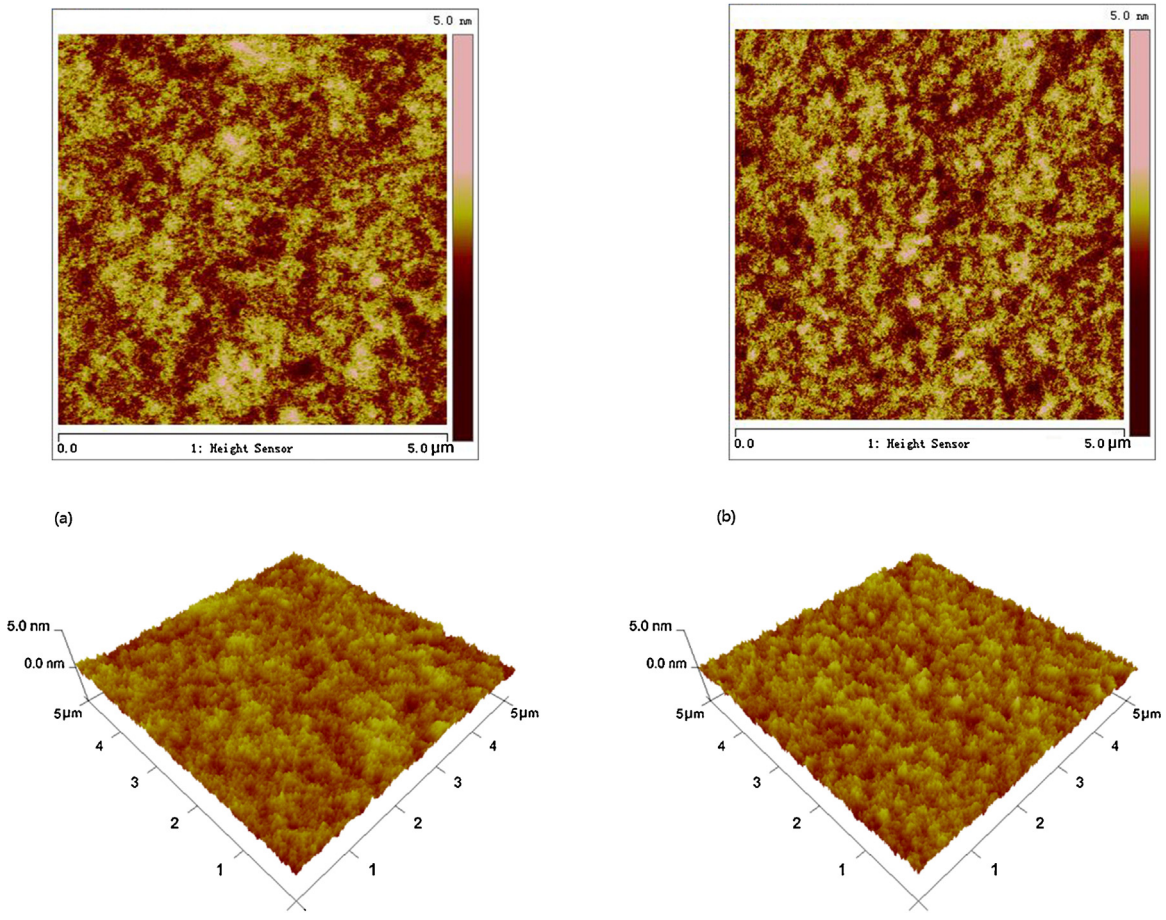

Fig. 9. Atomic force microscopy showing the morphology of SQ:$PC_{71}BM$ blend films (size 5 μm × 5 μm) for (a) un-annealing, and (b) annealing at 70 °C.

to diffuse to the donor–acceptor interface and charge carriers to transport to the respective electrodes after separation.

4. Conclusion

In summary, the anode modification and the thermal annealing were applied to optimize the performance of SQ:$PC_{71}BM$ based solution-processed solar cells. The results revealed that a maximum PCE of 4.08% was obtained through using MoO_3 as the anode modification layer and thermal annealing at 70 °C. CF_3CO_2H acid was used to prove that SQ is sensitive to acidic conditions and the acidic nature of PEDOT:PSS deteriorates the performance of OPVs based SQ:$PC_{71}BM$. MoO_3 layer acts as an effective exciton-blocking layer and improves the energy alignment between the anode and the active layer, finally enhances the PCE. The operation mechanism of the thermal annealing was straightened out. The higher carrier mobility and improved contact were obtained, which results from the improved nanoscale crystallinity and optimal scale of the phase separation after annealing. This work demonstrates the availability of anode modification and thermal annealing on small-molecule BHJ solar cells, which paves the way for further enhancing the PCE of small-molecule solar cells.

Acknowledgments

The authors express the thanks to the Research Fund for the Doctoral Program of Higher Education No. 20120009130005; the project supported by New Century Excellent Talents in University Grant No. NCET-10-0220; the Fundamental Research Funds for the Central Universities Grant No. 2012JBZ001; Excellent Doctor's Science and Technology Innovation Foundation of Beijing Jiaotong University (Grant No. 2013YJS091).

References

[1] G. Yu, J. Gao, J. Hummelen, F. Wudl, A. Heeger, Polymer photovoltaic cells: enhanced efficiencies via a network of internal donor–acceptor heterojunctions, Science 270 (1995) 1789.
[2] H.Y. Chen, J. Hou, S. Zhang, Y. Liang, G. Yang, Y. Yang, L. Yu, Y. Wu, G. Li, Polymer solar cells with enhanced open-circuit voltage and efficiency, Nature Photonics 3 (2009) 649–653.
[3] G. Li, R. Zhu, Y. Yang, Polymer solar cells, Nature Photonics 6 (2012) 153–161.
[4] S.H. Park, A. Roy, S. Beaupré, S. Cho, N. Coates, J.S. Moon, D. Moses, M. Leclerc, K. Lee, A.J. Heeger, Bulk heterojunction solar cells with internal quantum efficiency approaching 100%, Nature Photonics 3 (2009) 297–302.
[5] A.J. Moulé, K. Meerholz, Morphology control in solution-processed bulk-heterojunction solar cell mixtures, Advanced Functional Materials 19 (2009) 3028–3036.
[6] G. Wei, S. Wang, K. Renshaw, M.E. Thompson, S.R. Forrest, Solution-processed squaraine bulk heterojunction photovoltaic cells, ACS Nano 4 (2010) 1927–1934.
[7] F. Silvestri, M.D. Irwin, L. Beverina, A. Facchetti, G.A. Pagani, T.J. Marks, Efficient squaraine-based solution processable bulk-heterojunction solar cells, Journal of the American Chemical Society 130 (2008) 17640–17641.
[8] G. Chen, H. Sasabe, Z. Wang, X. Wang, Z. Hong, J. Kido, Y. Yang, Solution-processed organic photovoltaic cells based on a squaraine dye, Physical Chemistry Chemical Physics 14 (2012) 14661–14666.
[9] J. Xue, B.P. Rand, S. Uchida, S.R. Forrest, Mixed donor–acceptor molecular heterojunctions for photovoltaic applications. II. Device performance, Journal of Applied physics 98 (2005) 124903–124909.
[10] A. Benor, S.-y. Takizawa, C. Pérez-Bolívar, P. Anzenbacher Jr., Efficiency improvement of fluorescent OLEDs by tuning the working function of PEDOT:PSS using UV-ozone exposure, Organic Electronics 11 (2010) 938–945.
[11] M.D. Irwin, D.B. Buchholz, A.W. Hains, R.P. Chang, T.J. Marks, p-Type semiconducting nickel oxide as an efficiency-enhancing anode interfacial layer in polymer bulk-heterojunction solar cells, Proceedings of the National Academy of Sciences of the United States of America 105 (2008) 2783–2787.
[12] V. Shrotriya, G. Li, Y. Yao, C.-W. Chu, Y. Yang, Transition metal oxides as the buffer layer for polymer photovoltaic cells, Applied Physics Letters 88 (2006), 073508–073503.
[13] N. Li, B.E. Lassiter, R.R. Lunt, G. Wei, S.R. Forrest, Open circuit voltage enhancement due to reduced dark current in small molecule photovoltaic cells, Applied Physics Letters 94 (2009) 023307.
[14] Y. Sun, C.J. Takacs, S.R. Cowan, J.H. Seo, X. Gong, A. Roy, A.J. Heeger, Efficient air-stable bulk heterojunction polymer solar cells using MoOx as the anode interfacial layer, Advanced Materials 23 (2011) 2226–2230.
[15] Y. Long, Effects of metal electrode reflection and layer thicknesses on the performance of inverted organic solar cells, Solar Energy Materials and Solar Cells 94 (2010) 744–749.
[16] M. De Jong, L. Van Ijzendoorn, M. De Voigt, Stability of the interface between indium-tin-oxide and poly (3,4-ethylenedioxythiophene)/poly (styrenesulfonate) in polymer light-emitting diodes, Applied Physics Letters 77 (2000) 2255–2257.
[17] T. Nguyen, S. De Vos, An investigation into the effect of chemical and thermal treatments on the structural changes of poly (3,4-ethylenedioxythiophene)/polystyrenesulfonate and consequences on its use on indium tin oxide substrates, Applied Surface Science 221 (2004) 330–339.
[18] W. Ma, C. Yang, X. Gong, K. Lee, A.J. Heeger, Thermally stable, efficient polymer solar cells with nanoscale control of the interpenetrating network morphology, Advanced Functional Materials 15 (2005) 1617–1622.
[19] B. Walker, A.B. Tamayo, X.D. Dang, P. Zalar, J.H. Seo, A. Garcia, M. Tantiwiwat, T.Q. Nguyen, Nanoscale phase separation and high photovoltaic efficiency in solution processed, small molecule bulk heterojunction solar cells, Advanced Functional Materials 19 (2009) 3063–3069.
[20] T.S. van der Poll, J.A. Love, T.Q. Nguyen, G.C. Bazan, Non-basic high-performance molecules for solution-processed organic solar cells, Advanced Materials 24 (2012) 3646–3649.
[21] C. He, C. Zhong, H. Wu, R. Yang, W. Yang, F. Huang, G.C. Bazan, Y. Cao, Origin of the enhanced open-circuit voltage in polymer solar cells via interfacial modification using conjugated polyelectrolytes, Journal of Materials Chemistry 20 (2010) 2617–2622.
[22] V. Mihailetchi, P. Blom, J. Hummelen, M. Rispens, Cathode dependence of the open-circuit voltage of polymer: fullerene bulk heterojunction solar cells, Journal of Applied physics 94 (2003) 6849–6854.
[23] H. Azimi, A. Senes, M.C. Scharber, K. Hingerl, C.J. Brabec, Charge transport and recombination in low-bandgap bulk heterojunction solar cell using bis-adduct fullerene, Advanced Energy Materials 1 (2011) 1162–1168.
[24] Z. He, C. Zhong, X. Huang, W.Y. Wong, H. Wu, L. Chen, S. Su, Y. Cao, Simultaneous enhancement of open-circuit voltage, short-circuit current density, and fill factor in polymer solar cells, Advanced Materials 23 (2011) 4636–4643.
[25] V.D. Mihailetchi, J.K. van Duren, P.W. Blom, J.C. Hummelen, R.A. Janssen, J.M. Kroon, M.T. Rispens, W.J.H. Verhees, M.M. Wienk, Electron transport in a methanofullerene, Advanced Functional Materials 13 (2003) 43–46.
[26] N.F. Mott, R.W. Gurney, Electronic Processes in Ionic Crystals, Dover, New York, 1964.
[27] T. Erb, U. Zhokhavets, G. Gobsch, S. Raleva, B. Stühn, P. Schilinsky, C. Waldauf, C.J. Brabec, Correlation between structural and optical properties of composite polymer/fullerene films for organic solar cells, Advanced Functional Materials 15 (2005) 1193–1196.